Precipitation of rutile and ilmenite needles in garnet: Implications for extreme metamorphic conditions in the Acadian Orogen, U.S.A.

JAY J. AGUE[1,2,*] AND JAMES O. ECKERT JR.[1]

[1]Department of Geology and Geophysics, Yale University, P.O. Box 208109, New Haven, Connecticut 06520-8109, U.S.A.
[2]Peabody Museum of Natural History, Yale University, New Haven, Connecticut 06511, U.S.A.

ABSTRACT

We report the discovery of oriented needles of rutile and ilmenite in garnet crystals from granulite facies metapelitic rocks of the Merrimack synclinorium, Connecticut, and present a precipitation model for their origin. The rocks were strongly metamorphosed and deformed during the Devonian Acadian orogeny. The needles are primarily elongated parallel to <111> in garnet. Rutile has anomalous extinction angles as great as ~35° (cf. Griffin et al. 1971). Rutile and ilmenite needles are typically a few hundred nanometers to several micrometers in diameter and are several tens of micrometers to nearly a millimeter long. Other oxide inclusions that may be present include submicrometer- to micrometer-scale twinned rutile bicrystals, as well as srilankite and a crichtonite group mineral. Some garnet cores have unusual, box-shaped quartz inclusions, which coexist with Ti±Fe oxide needles and commonly contain micrometer-scale rods of F-OH-Cl apatite. Negative garnet crystal "pores" are also widespread. Ti±Fe oxide needles are restricted to garnet core regions; rims have a distinctly different inclusion population dominated by granulite facies minerals including sillimanite, spinel, cordierite, and K-feldspar. Consequently, the garnet core regions represent an earlier, distinct period of growth relative to the rims. Garnet cores contain ~25–35% pyrope, and a host of minor and trace constituents including TiO_2 (0.07–0.6 wt%), Cr_2O_3 (0.01–0.10 wt%), Na_2O (0.01–0.03 wt%), P_2O_5 (0.01–0.09 wt%), and ZrO_2 (up to ~150 ppm). Na_2O and ZrO_2 correlate positively with TiO_2. Titanium zoning is preserved in some garnets; zoning profiles and two-dimensional chemical mapping show that Ti and, to a lesser degree, Cr are depleted around Ti±Fe oxide inclusions. Therefore, we conclude that the needles are precipitates that formed from Ti-bearing garnet during exhumation and cooling. Garnet contained sufficient Ti to form precipitates; no Ti source external to garnet was necessary. Titanium-bearing garnets that contain oriented Ti±Fe oxide needles are known primarily from ultrahigh-pressure metamorphic rocks, mantle peridotites and pyroxenites, and high-pressure granulites. Thus, the presence of needle-bearing garnets in Connecticut strongly suggests that a previously unrecognized domain of extreme pressure and/or temperature metamorphism exists in the Acadian orogen.

Keywords: Metamorphic petrology, precipitates, rutile needles, ilmenite needles, high-pressure studies, high-temperature studies

INTRODUCTION

Oriented, needle-shaped inclusions of rutile or, less commonly, ilmenite that lie parallel to <111> in garnet have been found in rocks from a broad range of extreme pressure-temperature (*P-T*) environments, including: (1) ultrahigh-pressure (UHP) metamorphic rocks (Fig. 1a; e.g., Larsen et al. 1998; Zhang and Liou 1999; Ye et al. 2000; Mposkos and Kostopoulos 2001; Zhang et al. 2003; Barron et al. 2005; Griffin 2008); (2) mantle peridotites, pyroxenites, and xenocrysts (e.g., Obata 1994; Van Roermund and Drury 1998; Wang et al. 1999; Van Roermund et al. 2000a; Keshav and Sen 2001; Zhang and Liou 2003; Vrána 2008); and (3) granulite facies rocks formed at (ultra)high-*T* > ~900 °C, particularly high-*P* granulites (e.g., Snoeyenbos et al. 1995; O'Brien et al. 1997; Marschall et al. 2003; O'Brien and Rötzler 2003). Oriented rutile needles are also found in other ferromagnesian phases, including orthopyroxene (Moraes et al.

2002) and sagenitic biotite (Shau et al. 1991).

The Ti content of garnet increases with *T* and *P* (e.g., Khomenko et al. 1994; Ono 1998; Zhang and Liou 2003; Zhang et al. 2003; Kawasaki and Motoyoshi 2007). Therefore, it has been widely proposed that the needles form by precipitation from originally Ti-rich garnet during cooling and exhumation. However, Hwang et al. (2007), in their pioneering analytical electron microscope (AEM) study, concluded that rutile needles do not have a specific crystallographic relationship with their garnet hosts (all their studied rocks are now known to be UHP, including the granulites of the Bohemian Massif; Kotková et al. 2011). Exsolution via simple solid-state precipitation would favor continuity of crystal lattices across host-precipitate interfaces (coherency) and, thus, a specific crystallographic relationship between rutile and garnet (e.g., Putnis 1992). Consequently, the precipitation origin has been questioned in recent years. Alternative possibilities advanced by Hwang et al. (2007) include: (1) inheritance of needles from precursor phases; (2)
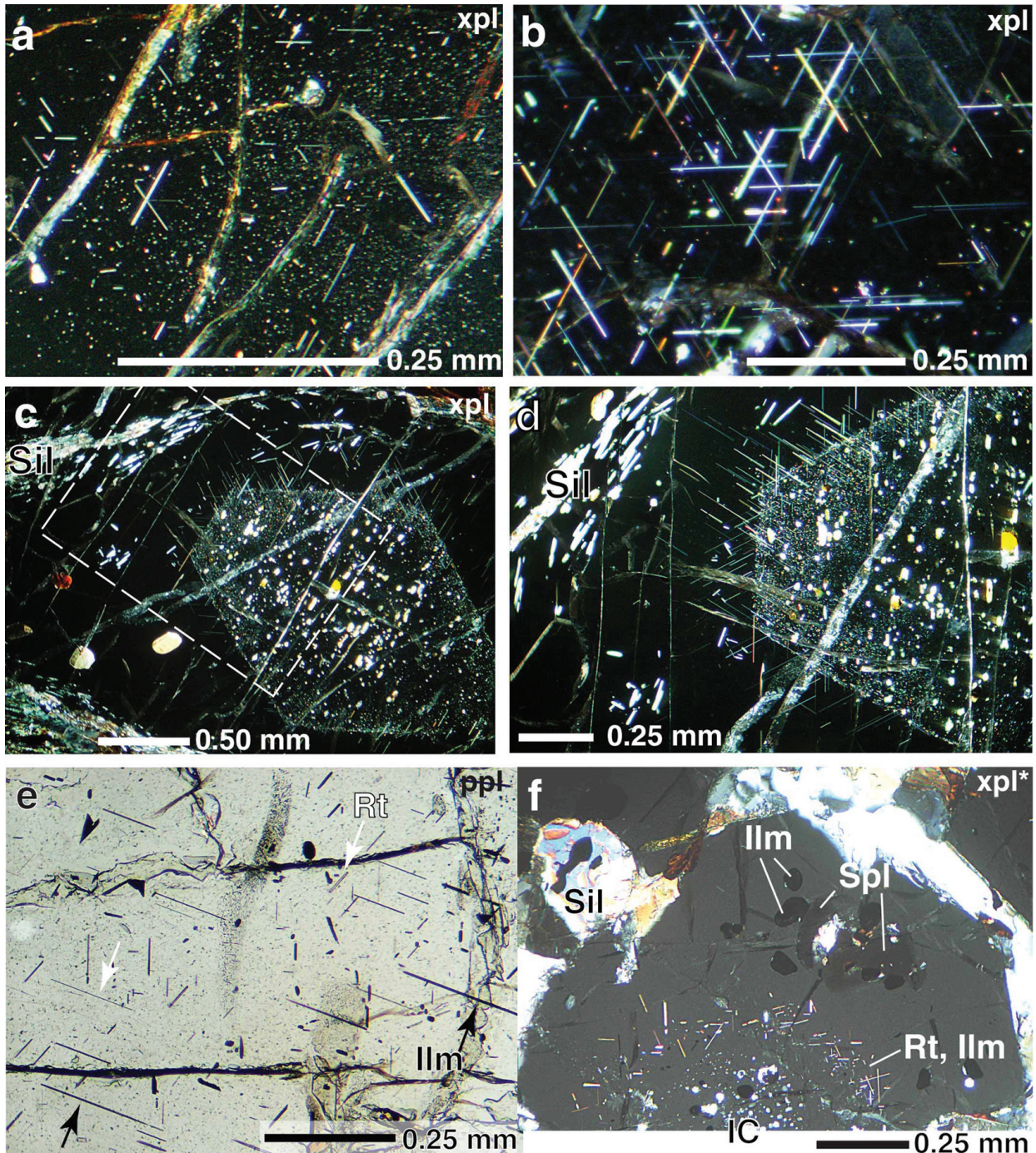
FIGURE 1. Photomicrographs of inclusions in garnet, conoscopic illumination. ppl = plane-polarized light; xpl = cross-polarized light. Specimen numbers in square brackets for this and all following figures. (**a**) Oriented rutile needles in diamondiferous gneiss, Saidenbach reservoir, Saxonian Erzgebirge [SB2]. Rock composed primarily of phengite, plagioclase, quartz, garnet, kyanite, rutile, and zircon. Bright spots are submicrometer- to micrometer-scale untwinned and twinned rutile plates (see Fig. 4). (**b**) Oriented rutile needles in garnet [5-5]. This and all other figure panels depict Connecticut rocks. (**c**) "Ghost" of earlier euhedral garnet outlined by rutile needles and microplates [58A-2]. Part (**d**) shows area enclosed by dashed rectangle. (**d**) Close-up of garnet in part **c**. Rutile inclusions become more abundant as the outer margin of the needle-rich zone is approached; most bright dots are rutile plates. Rim of garnet has many sillimanite (Sil) inclusions. Bright inclusions in core include quartz and tourmaline (yellow). (**e**) Ilmenite (Ilm, dark arrows) and rutile (Rt, white arrows) needles in garnet [5-4]. (**f**) Complex inclusion pattern in garnet photographed under partially crossed polarized light (xpl*) [68A]. Innermost core of garnet (IC) is rich in quartz inclusions. This is zone surrounded by an annulus of rutile and ilmenite needles. Outside this annulus in the rim, Ti±Fe oxide needles are absent, and spinel (Spl), sillimanite (Sil), and rounded ilmenite inclusions are found. These rim inclusions are typical of the granulite facies matrix, demonstrating that the rim grew over matrix phases. (Color online.)

a dissolution-reprecipitation mechanism; and (3) cleaving and healing of garnet synchronously with rutile crystallization. Of these, Hwang et al. (2007) favored (3), but also noted that none of the proposed mechanisms can fully explain observed garnet-rutile relationships.

In this paper, we describe a newly discovered locality for oriented rutile and ilmenite needles in garnet, and then use these rocks to test the precipitation hypothesis. The rocks are metapelites that form part of the Acadian orogen exposed in northeastern Connecticut, U.S.A. They contain the first documented occurrence of oriented needles in Acadian rocks of which we are aware. Oriented rutile inclusions have been reported farther west in the Taconic orogen in Massachusetts by Snoeyenbos and Koziol (2008) and Koziol and Snoeyenbos (2009). The precipitation hypothesis predicts that garnet in the vicinity of Ti±Fe oxides will be depleted in Ti, as Ti would need to diffuse from garnet to the precipitates as they grew. Chemical mapping and quantitative chemical analyses of inclusions and host garnet using the field emission gun electron probe microanalyzer (FEG-EPMA) demonstrate the existence of these depleted zones, consistent with the hypothesis that the needles precipitated from original Ti-bearing garnets. Such garnets can be important indicators of extreme P and/or T environments in the crust or mantle (cf. Zhang and Liou 1999; O'Brien and Rötzler 2003; Griffin 2008; Meinhold 2010). The potential presence of extreme P and/or T rocks in the New England Appalachians would have significant implications for our understanding of the petrotectonic evolution of the mountain belt (cf. Hacker et al. 2003; O'Brien and Rötzler 2003; Dobrzhinetskaya et al. 2007; Ernst and Liou 2008).

GEOLOGIC RELATIONS

Oriented Ti±Fe oxide needles have been discovered in the cores of garnet from the Brimfield Schist and Tatnic Hill Formation (Fig. 2). These rock units are part of the Merrimack synclinorium in northeastern Connecticut, which underwent deformation and peak metamorphism during the Devonian Acadian orogeny (e.g., Rodgers 1981; Robinson and Tucker 1982; Schumacher et al. 1989; Armstrong et al. 1992; Wintsch et al. 1992; Thomson 2001). Metapelitic rocks of the Brimfield Schist preserve granulite facies plagioclase+quartz+garnet+sillimanite± biotite±cordierite±K-feldspar±spinel mineral assemblages. The Tatnic Hill samples lack cordierite and spinel. Graphite, rutile, zircon, monazite, apatite, tourmaline, and pyrrhotite are common accessories. Although the pervasive high-grade metamorphism largely obliterated the prograde history of the rocks, widespread sillimanite pseudomorphs after kyanite attest to an earlier stage of metamorphism in the kyanite stability field (Peper and Pease 1975; Fahey and Pease 1977). Following high-grade metamorphism, the rocks were overprinted to varying degrees under kyanite zone conditions (e.g., Schumacher et al. 1989; Armstrong et al. 1992; Ague 1996; Thomson 2001). The rocks are strongly strained, and in some extreme cases have a protomylonitic texture.
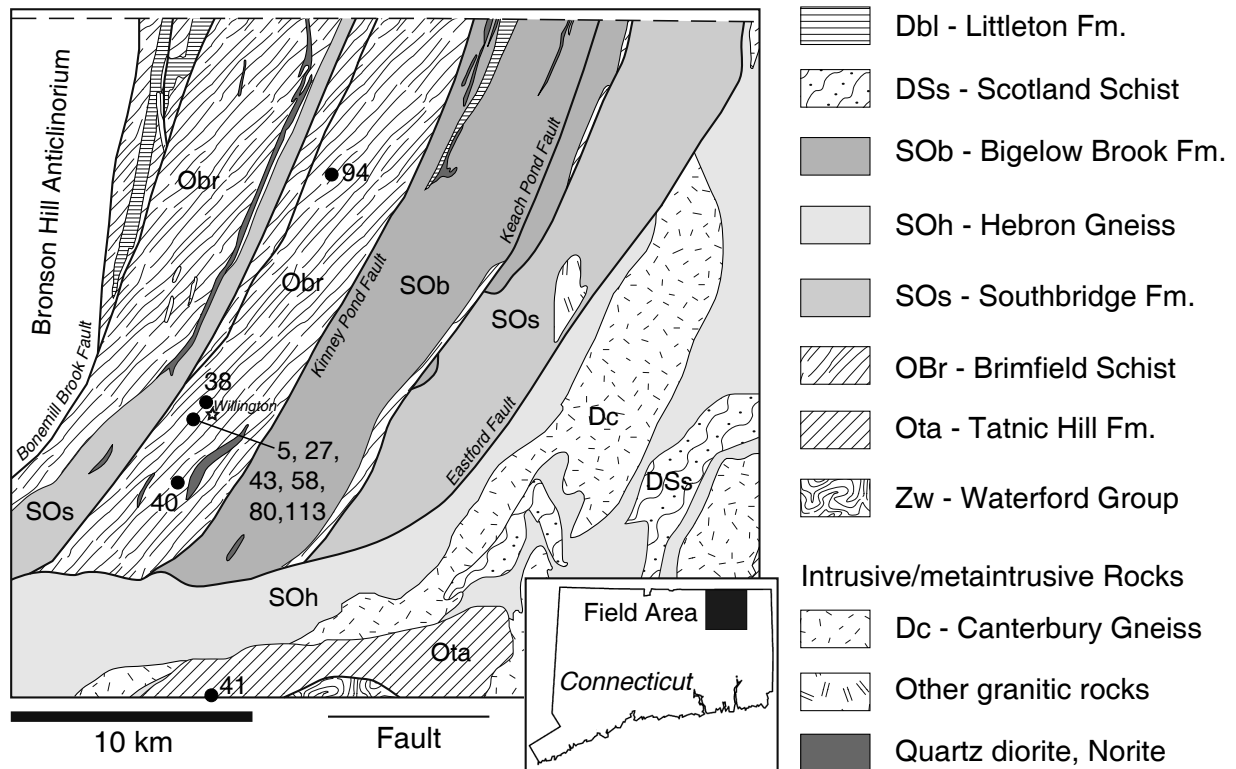

FIGURE 2. Simplified geologic map of part of the Merrimack synclinorium in northeastern Connecticut, after Rodgers (1981, 1985). Major west-dipping thrust faults are labeled. Sample localities with needle-bearing garnets denoted by filled circles; sample number prefix JAQ omitted for clarity.

Methods

Chemical maps, quantitative wavelength-dispersive spectrometer (WDS) analyses, energy-dispersive spectrometer analyses (EDS), and backscattered-electron (BSE) images were acquired using the JEOL-JXA 8530F field emission gun electron probe microanalyzer (FEG-EPMA) at Yale University. Quantitative "spot" analyses employed: 10 or 15 kV accelerating voltage; natural and synthetic standards; 10 nA (apatite), 100 nA (garnet), or 150 nA (oxides) beam currents; and off-peak background corrections. Trace elements were counted for long times (100–200 s on peak) to optimize counting statistics. Titanium and Zr counts were gathered with a high-reflectivity PETL crystal. An accelerating voltage of 10 kV was used for analyzing apatite and the Ti±Fe oxides, because the lower accelerating voltage yields a smaller activation volume. As a result, the low kV, in concert with the high-brightness field emission source, allowed quantitative analysis of crystals with minimum dimensions as small as ~800 nm. ZAF matrix corrections were employed for all phases, with the exception of Bence and Albee (1968) method corrections for garnet; these used custom α-factor tables supplied by the manufacturer (at 15 kV). As has been widely observed, ZAF corrections commonly yield anomalously high totals for garnet (102–104 wt%), most likely as a result of uncertainties on matrix correction factors for Mg-rich, Fe-bearing silicates. We emphasize that concentrations of minor and trace elements in garnet are insensitive to the matrix correction procedure used. Chemical mapping of Ti in garnet was done with 15 kV accelerating voltage, 150 ms dwell time, and 200 nA beam current.

Analytical reproducibility values (sample standard deviation, $\pm 1\sigma$) based on 30 replicate analyses of homogeneous garnet in sample JAQ-5-1 are (wt%): SiO_2 = $\pm$0.12; TiO_2 = $\pm$0.002; ZrO_2 = $\pm$0.002; P_2O_5 = $\pm$0.004; Al_2O_3 = $\pm$0.20; Cr_2O_3 = $\pm$0.004; FeO = $\pm$0.13; MgO = $\pm$0.06; MnO = $\pm$0.03; CaO = $\pm$0.02; Na_2O = $\pm$0.003. These are considered conservative as: (1) the garnet may have some internal zonation and (2) the uncertainty on mean values (standard error) is smaller by a factor of $\sqrt{N}$, where N is the number of individual analyses. A similar treatment of results from rutile in sample JAQ-113Ad yields (wt%): SiO_2 = $\pm$0.01; TiO_2 = $\pm$0.48; ZrO_2 = $\pm$0.006; Al_2O_3 = $\pm$0.01; Cr_2O_3 = $\pm$0.01; Nb_2O_5 = $\pm$0.19; Ta_2O_5 = $\pm$0.01; V_2O_5 = $\pm$0.03; FeO = $\pm$0.14; MnO = $\pm$0.01; MgO = $\pm$0.002.

Rectangular grids of spot analyses were done to estimate garnet bulk Ti contents in several garnet cores that contain Ti±Fe oxide needles (e.g., Hacker et al. 1997). To obtain comprehensive coverage, a wide beam (20 μm) was used together with analysis points spaced 20 μm apart. The number of analysis points for grids in samples 5-1, 5-4, and 27-1 were 144, 284, and 144, respectively.

Petrographic relationships

Needle-bearing garnets are typically a few millimeters to about 1 cm in diameter, and have a distinctive pink-lavender color. They are rich in pyrope (~25–35%) and almandine, but poor in grossular and spessartine (Table 1). The oxide needles occupy garnet cores and are predominantly oriented along <111> in garnet, as observed in other settings worldwide (Fig. 1; see Introduction). This orientation precludes inheritance of needles from sagenitic biotite (Shau et al. 1991; Hwang et al. 2007).

Rutile generally predominates; proportions range from subequal amounts of rutile and ilmenite (Fig. 1e), to all rutile with no ilmenite. Ilmenite and rutile needles are similar in size and shape (Figs. 1 and 3). They range in diameter from a few hundred nanometers to a few micrometers, and can reach nearly 1 mm in length. Needles are largest and most abundant near the town of Willington, and are less conspicuous at the southern and northern localities (Fig. 2).

The rutile needles are characterized by anomalous extinction, identical to that reported by Griffin et al. (1971) in eclogites from kimberlites and the Western Gneiss Region, Norway. Rutile is tetragonal, so the needles would be expected to go to extinction parallel to the crosshairs under cross-polarized light. However, a wide range of extinction angles is observed—from 0° to ~35°. Even perfectly parallel needles directly adjacent to each other can have different extinction angles. The variability of crystallographic axis orientation in rutile needles relative to

TABLE 1. Garnet (Grt) and apatite (Ap) analyses

	Grt 5-1 Rim	Grt 5-1 Core	Grt 5-4 Core	Grt 38D Core	Grt 43A-1 Core	Grt 58A-1 Core	Ap 27-1 no. 1	Ap 27-1 no. 2
SiO_2	38.41	38.71	37.70	38.06	38.32	38.42	0.12	0.38
TiO_2	0.014	0.072	0.581	0.252	0.372	0.073	0.05	b.d.
ZrO_2	b.d.	0.006	0.015	b.d.	0.016	0.001		
P_2O_5	0.037	0.077	0.029	0.007	0.048	0.030	40.81	40.89
Al_2O_3	21.55	21.68	21.22	21.12	21.28	21.32	0.05	0.09
Cr_2O_3	0.04	0.09	0.04	0.02	0.06	0.01		
Y_2O_3	b.d.	b.d.	0.06	0.12	0.02	0.06		
FeO	30.83	28.88	29.33	30.31	29.49	30.01	1.27	1.67
MgO	7.27	8.87	7.84	6.98	7.51	7.10	0.08	0.06
MnO	0.95	0.98	1.16	0.78	1.10	1.32	0.12	0.09
ZnO					0.03	0.02		
CaO	1.45	1.32	1.24	1.52	1.31	1.25	54.21	52.45
Na_2O	0.004	0.014	0.026	0.016	0.011	0.010	0.07	0.12
F							2.21	1.92
Cl							0.49	0.49
Total	100.56	100.70	99.25	99.18	99.57	99.62	98.44	97.24

	Garnet (12 O)						Apatite (12.5 O)	
Si	2.988	2.976	2.965	3.002	2.999	3.012	0.010	0.033
Ti	0.0008	0.0042	0.0344	0.0149	0.0219	0.0043	0.003	
Zr·10		0.0022	0.0058		0.0061	0.0004		
P	0.0024	0.0050	0.0019	0.0005	0.0032	0.0020	2.954	2.977
^{IV}Al	0.012	0.024	0.035		0.001			
^{VI}Al	1.964	1.941	1.922	1.964	1.963	1.970		
Al^{Total}	1.976	1.965	1.957	1.964	1.964	1.970	0.005	0.009
Cr	0.002	0.005	0.003	0.001	0.004	0.001		
Y			0.003	0.005	0.001	0.002		
Fe^{2+}	1.973	1.807	1.888	1.979	1.919	1.943	0.091	0.120
Fe^{3+}	0.033	0.050	0.041	0.020	0.011	0.025		
Mg	0.843	1.016	0.919	0.820	0.876	0.830	0.010	0.008
Mn	0.063	0.064	0.077	0.052	0.073	0.088	0.009	0.007
Ca	0.121	0.109	0.105	0.128	0.110	0.105	4.966	4.833
Na	0.0006	0.0021	0.0040	0.0024	0.0017	0.0015	0.012	0.020
F							0.598	0.522
Cl							0.071	0.071
OH							0.331	0.407

Notes: b.d. = below detection. Blank in wt% table means element or oxide not analyzed. Fe^{2+} and Fe^{3+} in garnet estimated based on 2 octahedral sites per 12 O. By convention, garnet ^{IV}Al is amount needed to fill the tetrahedral sites; however, actual site occupancies have not been determined. 5-4 is the average of 284 analysis points acquired on a wide-beam analysis grid. OH in apatite structural formulas computed by difference assuming one (F^-,Cl^-,OH^-) site. Oxygen equivalent of F^- and Cl^- subtracted from apatite totals. Zr·10 is Zr moles multiplied by 10.

elongation direction was verified by the AEM measurements of Hwang et al. (2007).

Several other morphologies besides needles can be present. For example, submicrometer- to micrometer-scale plates of rutile, which are commonly twinned, are found in some garnets (Fig. 4). These are morphologically similar to twinned bicrystals found in the diamondiferous UHP Saxonian Erzgebirge rocks (Hwang et al. 2000). Hwang et al. showed that the Erzgebirge twins were separated by nanometer-scale α-PbO_2-type TiO_2 stable at P ~4–5 GPa or more; we have not determined if the α-PbO_2 structure is present in our bicrystals. "Blocky" ilmenite-zircon intergrowths are also observed (Fig. 3e).

Inclusions of the rare oxides srilankite (Ti_2ZrO_6) and a crichtonite group mineral are notable (Figs. 3c and 3d; Table 2). Unlike srilankite, the compositions of minerals in the crichtonite group are extremely variable and solid solution is extensive (e.g., Wang et al. 1999); 14 group members are currently recognized. Analyses indicate the presence of loveringite ([Ca,Ce][Ti,Fe,Cr,Mg]$_{21}$O$_{38}$) and davidite-(Ce) ([Ce,La][Y,U,Fe][Ti,Fe]$_{21}$O$_{38}$) components, among others (Table 2). Srilankite is more common than crichtonite in the garnets, but neither phase is abundant. Textural relations are complex and often include
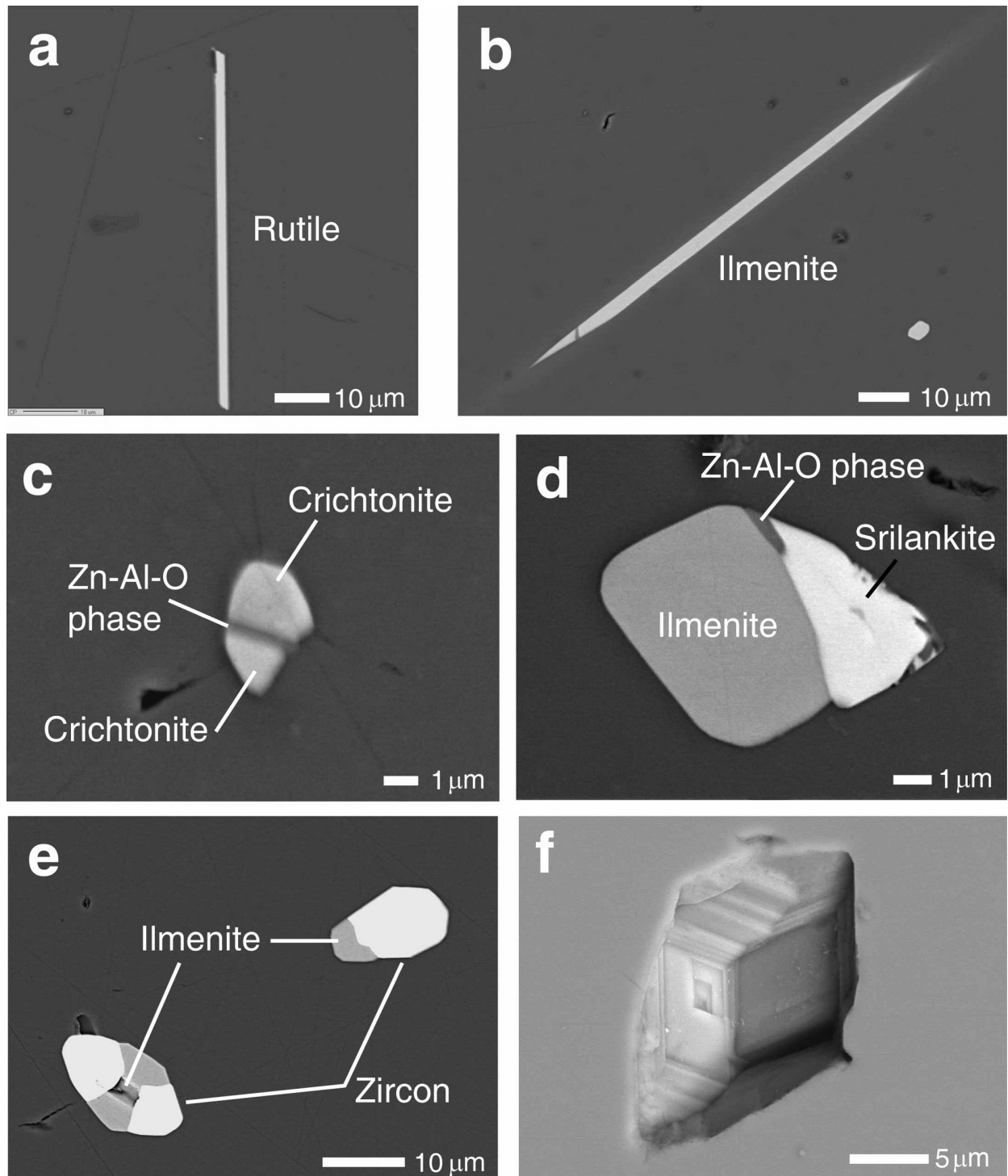
FIGURE 3. Backscattered electron images of inclusions in garnet. (**a**) Rutile needle [5-2]. (**b**) Ilmenite needle [5-4]. (**c**) Two crichtonite plates, separated by Zn-Al-O phase [5-4]. (**d**) Ilmenite and srilankite with small region of intervening Zn-Al-O phase [5-4]. (**e**) Composite ilmenite-zircon inclusions [5-1]. (**f**) Pore with internal negative garnet crystal facets [80A].
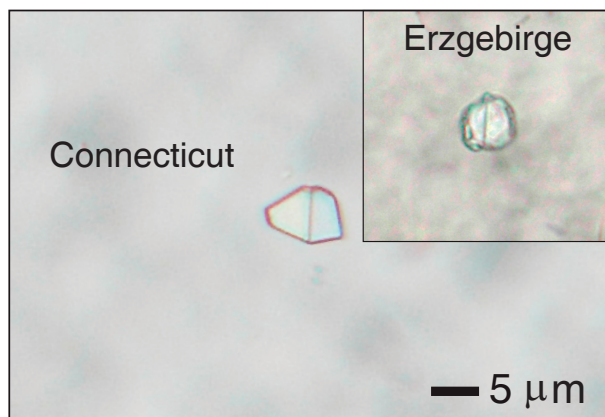
FIGURE 4. Twinned rutile bicrystal inclusion in garnet from Connecticut [5-3]. Inset shows similar-appearing example from diamondiferous gneiss, Saxonian Erzgebirge [SB2]. Scale bar applies to both photomicrographs. Plane-polarized light. (Color online.)

multiple phases. For example, Figure 3c shows two crichtonite plates separated by a ~500 nm wide zone of a second phase. Energy-dispersive chemical analysis indicates that the second phase is composed mostly of Zn, Al, and O, suggesting that it is the spinel gahnite. Further work would be needed to confirm this. Figure 3d shows the Zn-Al-O phase present between plates of srilankite and ilmenite.

TABLE 2. Oxide analyses

	Rt 5-1 no. 3-1	Rt 5-4 no. 2-1	Rt 27-1 no. 1-17	Ilm 5-1 no. 2-1	Ilm 5-3 no. 1-4	Ilm 5-3 no. 2	Sri 5-3 no. 3	Sri 5-4 no. 1	Cri 5-4 no. 1
SiO_2	0.15	0.08	0.11	0.07	0.05	0.06	0.27	0.17	0.28
TiO_2	97.64	95.99	92.27	53.02	53.29	52.82	55.10	53.38	60.32
ZrO_2	0.028	0.306	0.887	0.027	b.d.	b.d.	42.10	44.15	5.65
Al_2O_3	0.08	0.03	0.05	0.02	0.03	0.03	0.25	0.11	4.23
Cr_2O_3	0.02	0.05	0.02	0.04	b.d.	0.03	b.d.	b.d.	0.30
Nb_2O_5	0.16	0.55	2.72	b.d.	b.d.	0.01	0.09	0.16	0.02
Ta_2O_5	0.03	0.02	0.05	0.01	b.d.	0.02	b.d.	b.d.	b.d.
V_2O_5		1.09	2.15		0.21		0.15	0.02	3.16
Fe_2O_3	1.62	1.50	2.19	1.09	0.60	1.65			
FeO				43.39	43.82	43.43	2.05	1.86	18.03
MnO	0.05	0.04	0.06	0.27	0.23	0.29	0.08	b.d.	0.08
MgO	0.02	0.01	0.01	2.32	2.21	2.18	0.04	0.01	0.82
Total	99.80	99.67	100.52	100.26	100.44	100.52	100.13	99.86	99.80*
Structural formulas									
Si	0.002	0.001	0.002	0.002	0.001	0.002	0.013	0.008	0.081
Ti	0.983	0.968	0.930	0.987	0.991	0.982	1.956	1.917	13.172
Zr		0.002	0.006				0.969	1.028	0.800
Al	0.001	0.001	0.001	0.001	0.001	0.001	0.014	0.006	1.447
Cr		0.001		0.001		0.001			0.069
Nb	0.001	0.003	0.017				0.002	0.004	0.003
Ta									
V		0.010	0.019		0.004		0.005	0.001	0.606
Fe^{2+}				0.898	0.906	0.898	0.081	0.074	4.377
Fe^{3+}	0.016	0.015	0.022	0.020	0.011	0.031			
Mn	0.001	0.001	0.001	0.006	0.005	0.006	0.003		0.020
Mg				0.086	0.082	0.080	0.003	0.001	0.355

Notes: b.d.= below detection. Blank in wt% table means oxide not analyzed. Rt = rutile, Ilm = ilmenite, Sri = srilankite, Cri = crichtonite. All Fe as Fe_2O_3 for rutile and as FeO for srilankite and crichtonite. Structural formulas calculated on the basis of 2, 3, 6, and 38 O atoms for rutile, ilmenite, srilankite, and crichtonite, respectively. FeO and Fe_2O_3 for ilmenite calculated using two cations per three O atoms. V counts corrected for Ti interference; Cr counts corrected for V interference.
* Includes the following wt% values: ZnO = 1.33; SrO = 0.09; CaO = 1.08; BaO = 0.15; Na_2O = 0.25; K_2O = 0.07; HfO_2 = 0.03; La_2O_3 = 0.61; Ce_2O_3 = 2.64; UO_2 = 0.66.

The garnet cores contain a rich spectrum of other inclusions as well. Rounded, drop-like crystals of zircon, baddeleyite, Nd-monazite, monazite, and xenotime are relatively common. Rods and, more rarely, plates of apatite can also be found, often in close association with quartz inclusions (Fig. 5). In addition, other phosphates may coexist with the apatite and quartz (Fig. 5e). The apatite structural formula calculations indicate considerable OH⁻; mole fractions (X) are approximately: $X_F \approx 0.5–0.6$, $X_{OH} \approx 0.3–0.4$, and $X_{Cl} \approx 0.05–0.1$ (Table 1). The quartz inclusions are widespread in many garnet cores. They commonly have an unusual "boxy" appearance and are crudely aligned with each other (Fig. 5). Some quartz inclusions also contain tiny rutile needles (Fig. 5e). We have observed similar-appearing quartz and apatite crystals together with rutile needles in a sample of kyanite-garnet gneiss from the famous Fjørtoft UHP locality in Norway (Fig. 5f) (e.g., Dobrzhinetskaya et al. 1995; Robinson et al. 2003).

Another very common feature is pore space. It generally takes the form of "negative" garnet crystals a few micrometers to a few tens of micrometers across (Fig. 3f). Presumably these pores are or were filled with fluid (e.g., Frezzotti et al. 2011); this possibility will be explored in future papers. Negative crystal fluid inclusions are well known in minerals such as quartz (e.g., Kvenvolden and Roedder 1971). In addition, many pores are partially or completely filled by solid phases, including various combinations of magnesite–siderite solid solutions, pyrophyllite, quartz, Na-bearing phlogopite, aluminous talc, phengite, graphite, rutile, ilmenite, an Al_2SiO_5 phase, zircon, apatite, monazite, xenotime, calcite, and smithsonite.

Pyroxene is uncommon; nonetheless, one rod-like orthopyroxene inclusion was found together with rutile needles in JAQ-5-2.

The inclusion assemblages in the needle-bearing garnet cores contrast markedly with those in the rims. In some examples, the transition from core to rim is gradual; the needles become smaller and less abundant as the rims are approached. In other examples, a relatively sharp boundary separates core and rim (Figs. 1c, 1d, and 1f). In these cases, it is not uncommon to find that the highest concentration of needles is localized in a zone that runs along core–rim contacts (Figs. 1c and 1d). In some rocks, an inner core rich in quartz inclusions is ringed by Ti±Fe oxide needles (Fig. 1f).

The rim portions of garnets have inclusions that reflect growth over granulite facies matrix minerals. Sillimanite is extremely common, but cordierite, spinel, K-feldspar, and biotite inclusions are also widespread (Figs. 1d and 1f). The absence of Ti±Fe oxide needles/plates and negative garnet crystal pores from these rim zones is striking. Rarely, some needles extend out to where the sillimanite inclusions begin, but any overlap, if present, is minor and amounts to only a few micrometers or tens of micrometers at most. Critically, primary sillimanite, biotite, cordierite, K-feldspar, or spinel inclusions are *never* found in garnet cores together with Ti±Fe oxide needles. Biotite can sometimes be found, but in nearly all cases it is linked to the matrix by cracks and can be easily shown to post-date the needle-bearing cores. The above relationships clearly establish that the garnet core regions represent an earlier, distinct period of growth relative to the rims.
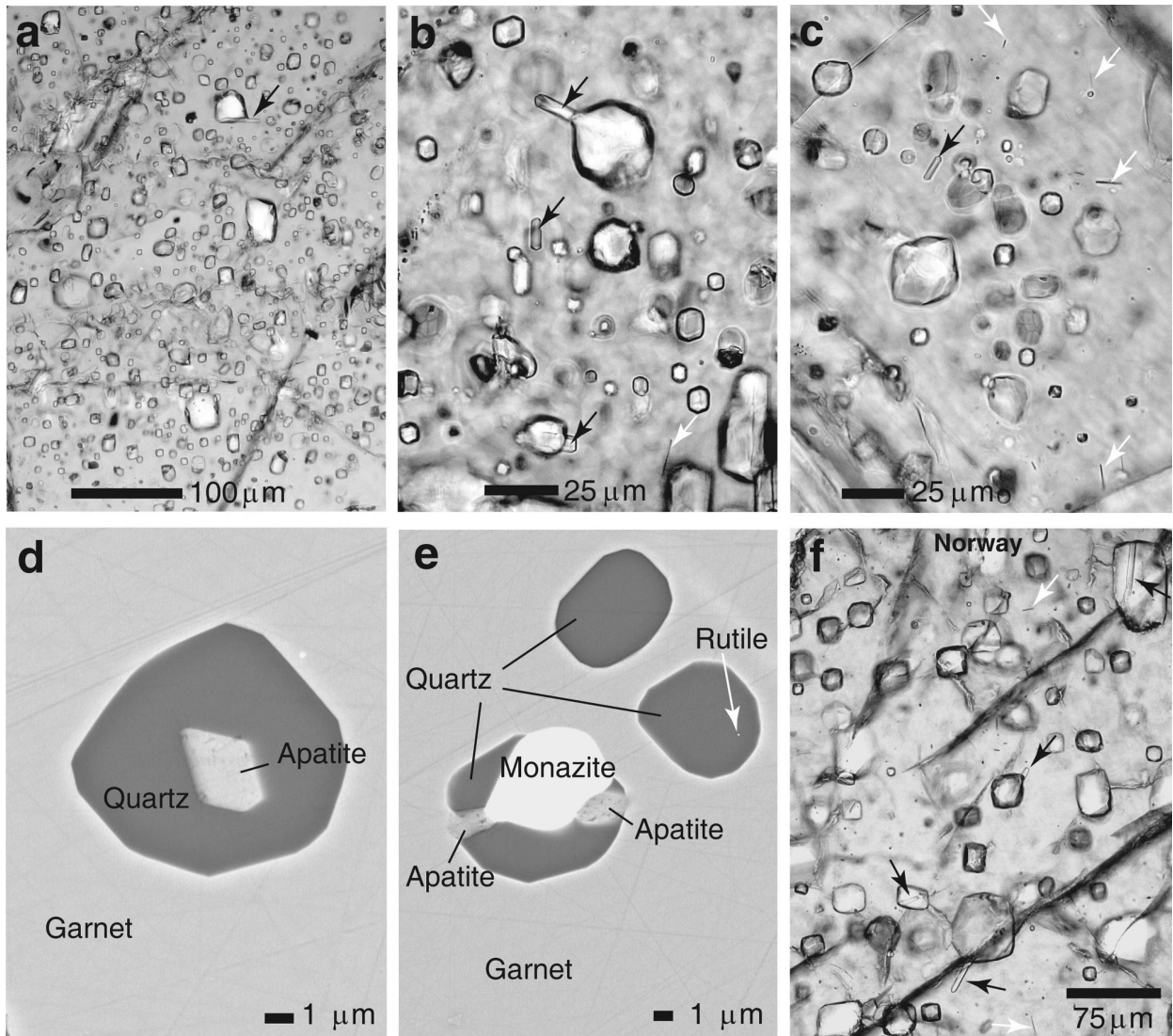
FIGURE 5. Quartz and apatite inclusions. (**a**–**c** and **f**) Plane-polarized light photomicrographs taken using conoscopic illumination. Black arrows denote apatite rods, white arrows denote rutile needles. (**d** and **e**) Backscattered electron images. (**a**) "Boxy" quartz inclusions in garnet core [27-2]. (**b**) Apatite rods and quartz inclusions [27-2]. Quartz and apatite are commonly found together in the same inclusion. Rutile needle at lower right. (**c**) Quartz, apatite rod, and rutile needles together in garnet core [27-2]. (**d**) Cross section through euhedral apatite rod in quartz inclusion [27-1]. (**e**) Complex quartz inclusion containing apatite and monazite [27-1]. Adjacent quartz inclusion contains rutile needle (white arrow). (**f**) Similar-appearing quartz and apatite inclusions from UHP kyanite-garnet gneiss, Vågholmen, Fjørtoft, Norway (stop 4-4 in Robinson et al. 2003).

We note that tiny, rare, sparsely distributed needles of rutile a few micrometers long or less, as well as submicrometer-scale plates of rutile, can be found in some lower-grade rocks. For example, such crystals are present in a few garnets from staurolite-kyanite zone rocks of the Wepawaug Schist, Connecticut (unpublished observations; see Ague 1994, 2011, and references therein for discussion of this rock unit). However, the needles are far smaller and far less abundant than those reported herein. Indeed, they are detectable only with very careful optical examination at high magnification, unlike the very obvious Ti±Fe oxides shown in Figure 1. They also lack the strong preferred shape orientation parallel to garnet <111>. The small size of the inclusions makes optical examination difficult; the presence

or absence of anomalous extinction could not be confidently ascertained.

OXIDE COMPOSITIONS AND GARNET ZONING

Oxide compositions

Representative oxide compositions are given in Table 2. Rutile needles contain variable amounts of minor and trace elements including V, Ta, Nb, Cr, and Zr. The Zr content of rutile coexisting with quartz and zircon is a sensitive thermometer (Zack et al. 2004; Watson et al. 2006; Tomkins et al. 2007). The needles preserve a large range of ZrO_2 concentrations, from several hundred parts per million to levels in the weight percent

range (Table 2). The temperature and petrogenetic significance of the rutile Zr contents will be addressed in a separate contribution. Ilmenite is relatively pure; structural formula calculations detect minor Fe_2O_3. Srilankite approaches the ideal formula of Ti_2ZrO_6, whereas crichtonite includes a wide range of minor and trace constituents including Zr, Ce, La, and U.

Garnet zoning and oxide precipitates

Some Ti±Fe oxide-bearing garnets retain Ti compositional zoning. This is well illustrated by garnets at locality JAQ-5. At this locality, Ti is highest in garnet cores, where needles are present, and drops smoothly toward rims, where needles are absent (Fig. 6a). Chromium and Mg/Fe behave similarly (Figs. 6b and 6c). The dip in Ti content at ~720 μm along the profile is discussed further below. The P profile is characterized by a sharp change in concentration at ~150 μm along the profile, which we conclude represents original chemical growth zoning (Fig. 6d). Maximum P_2O_5 concentrations reach ~0.09 wt%. Importantly, rutile needles are present in the high-phosphorous core of the garnet, but absent in the low-phosphorus rim. Total Al increases toward the rim, in contrast to Ti and Cr, which decrease (Fig. 6e).

The retention of sharp P discontinuities demonstrates extremely slow rates of diffusion, as observed for P in olivine (e.g., Mallmann et al. 2009). The smooth drops in Mg/Fe toward rims almost certainly reflect retrograde diffusional exchange with matrix biotite and/or cordierite. The shapes of the Ti and Cr profiles are similar and also suggest some degree of retrograde diffusion. This interpretation is bolstered by the P zoning, which shows that sharp discontinuities in composition could be produced during garnet growth, but were retained only for elements with exceedingly small diffusion coefficients. Moreover, the rock matrix contains abundant rutile + ilmenite and, thus, Ti was not limited during garnet growth. Consequently, it is highly unlikely that the observed core-to-rim Ti zoning was the result of Rayleigh fractionation. The original Ti profile cannot be reconstructed given available information, but it could have originally featured a sharp step like the P profile, which then diffusively relaxed over time.

A striking aspect of the profile is the Ti-depleted region that surrounds a rutile needle at ~720 μm (Fig. 6a). This phenomenon was explored further on a traverse that cuts diagonally through the garnet illustrated in Figures 7 and 8. The diagonal traverse was chosen as it intersects several oxide inclusions. These inclusions are surrounded by obvious Ti-depletion haloes (Fig. 7a). Furthermore, Cr depletion haloes surround the largest inclusions (Fig. 7c). The widest depleted zone at ~300 μm surrounds a blocky ilmenite-zircon intergrowth (see Figs. 3e, 7a, and 7c).

A two-dimensional chemical map of Ti in garnet is presented in Figure 8. It clearly shows the Ti-depletion haloes that surround oxide inclusions. Larger inclusions and clustered groups of inclusions tend to have the largest haloes. Needles are absent from the rim region; here, bulk garnet Ti contents are lower than in the core. The low-Ti haloes cannot be artifacts caused by areal excitation due to beam overlap onto adjacent oxide crystals or secondary Ti fluorescence, as these would result in artificially high, not low, apparent concentrations.

The profiles and map provide extremely strong evidence that the rutile and ilmenite inclusions in garnet cores are precipitates

that formed from Ti-bearing garnet. The shapes of the concentration profiles are consistent with diffusion from garnet to the inclusions during precipitation (e.g., at ~190 and ~300 μm in Fig. 7a).

By modeling the expected diameter of the Ti-depleted haloes and comparing the result with observations, the precipitation hypothesis can be further tested. We assume that the mass transfer from garnet to a rutile needle is by radial diffusion that affects a cylindrical zone in garnet surrounding the needle. The diffusion equation in cylindrical coordinates is

$$\frac{\partial C}{\partial t} = \frac{D}{r} \frac{\partial}{\partial r} \left(r \frac{\partial C}{\partial r} \right) \tag{1}$$

where D is the diffusion coefficient (taken to be constant), C is concentration, r is radial position, and t is time. D and, thus, the time needed for Ti diffusion in garnet are unknown, but this does not affect conclusions about length scales of Ti depletion. By specifying the mass of Ti needed to form a cylindrical rutile needle, one can easily compute the radius of the corresponding Ti-depleted zone in the surrounding garnet. For the garnet in Figures 7 and 8, the concentration of Ti distal to the needles averages 3.51×10^{-5} mol/cm³; this value was used as the initial model concentration. The rutile is taken to be pure (0.053 Ti mol/cm³). The interface with the needle is specified at $r = 0$, and the boundary concentration of Ti in garnet is held at zero for the duration of the simulation. Importantly, the length-scale results are little affected by the boundary concentration value. Equation 1 was solved using the forward time, centered space finite difference method (e.g., Thomas 1995). The value of D is arbitrary and was chosen for ease of numerical solution.

The sizes of model depletion haloes expected for representative 0.25–1 μm radius needles are shown in Figure 9. The characteristic radial depletion length scales of ~50 to ~100 μm correspond well with the observed halo dimensions in Figures 7 and 8. Consequently, Ti diffusion to needles can readily account for the Ti-depleted halo regions in garnet. We recognize that the growth of needles is inherently three dimensional and more complicated than the simple radial model we present. Nonetheless, there is no evidence that any Ti source external to garnet was needed to form the needles, although the possibility exists that other, more rapidly diffusing, elements were exchanged with the matrix (e.g., Proyer et al. 2009).

Rutile and ilmenite also contain Cr, which accounts for the Cr depletion haloes (Table 2; Fig. 7c). The Ti±Fe oxides contain relatively small amounts of Cr, so the Cr haloes are significantly narrower than the Ti haloes (the maximum Cr_2O_3 we measured in rutile is ~0.3 wt%). Some diffusion of Fe must have occurred to produce ilmenite, but protracted metamorphism at granulite facies conditions probably smoothed Fe zoning so that Mg/Fe shows no significant variation around needles (Figs. 6 and 7).

DISCUSSION

The Ti depletion haloes surrounding Ti±Fe oxide needles and plates leave little doubt that they are precipitates that formed from Ti-bearing garnet. The relatively smooth core-to-rim Ti zoning profiles suggest diffusional modification of primary growth zoning, probably during exhumation and cooling (Fig. 6a). When solid-state diffusion through the crystal lattice slowed as T continued to decrease, then shorter length-scale diffusion
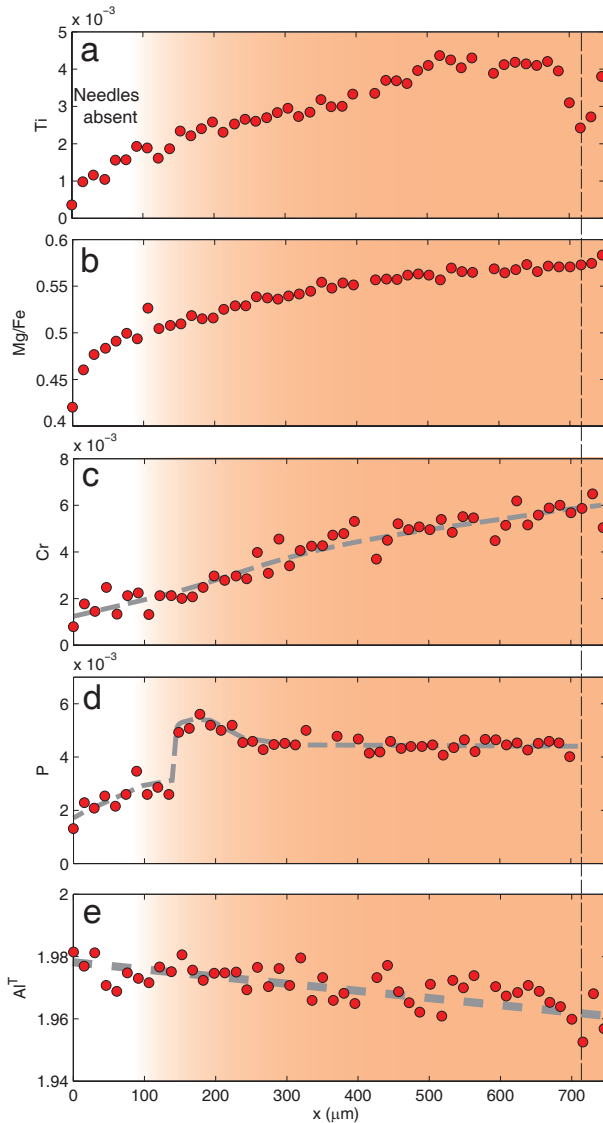
FIGURE 6. Chemical zoning profiles from core (right side) to rim (left side) across garnet [5-1]. Formula units plotted on 12 oxygen basis. The position of the rutile needle intersected by the traverse is denoted by vertical dashed line. Needles are present throughout the garnet in the shaded area, but are absent from the rim. (**a**) Ti. Note drop in Ti concentration around the rutile needle. (**b**) Mg/Fe. (**c**) Cr. (**d**) P. (**e**) Al^T (total aluminum). Al^T decreases as Ti and Cr increase. (Color online.)

FIGURE 7. Chemical zoning profiles that cut diagonally across the garnet shown in Figure 8. Formula units plotted on the basis of 12 O atoms. Positions of rutile needles and ilmenite-zircon inclusion shown with vertical dashed lines. Ilmenite-zircon inclusion at $x \approx 300$ µm (see Fig. 3e). Rim of garnet is toward right, but profile is not radial. (**a**) Ti. Note drop in Ti concentration around oxide inclusions. (**b**) Mg/Fe. (**c**) Cr. Note drop in Cr around oxide inclusions at $x \approx 190$ µm and $x \approx 300$ µm. (**d**) P. (**e**) Al^T (total aluminum). (Color online.)

and segregation of Ti occurred to form precipitates and relieve supersaturation in garnet. The <111> directions defined by the intersections among {110} parting planes in garnet could have been preferentially exploited by the precipitates during growth. The rates of Ti diffusion remain to be quantified, but they were slow enough to preserve Ti-depleted haloes around oxide inclusions, even during granulite facies metamorphism (Figs. 6–8). Slow Ti diffusion has been inferred for other ferromagnesian silicates as well, such as clinopyroxene (e.g., Proyer et al. 2009).

Incoherent and coherent precipitation

The atomic-scale mechanism of needle precipitation has not been determined, but we offer some general comments on the problem. The preferred orientation of needles along <111> in garnet is characteristic. In addition, the lateral sides of rutile needles are bounded by the lowest energy {110} planes of garnet, and in most cases the growth directions are close to the normal of {101} planes of rutile (Hwang et al. 2007). We note that Figure 3 of Hwang et al. (2007) shows that one of the *a*-axes in the seven
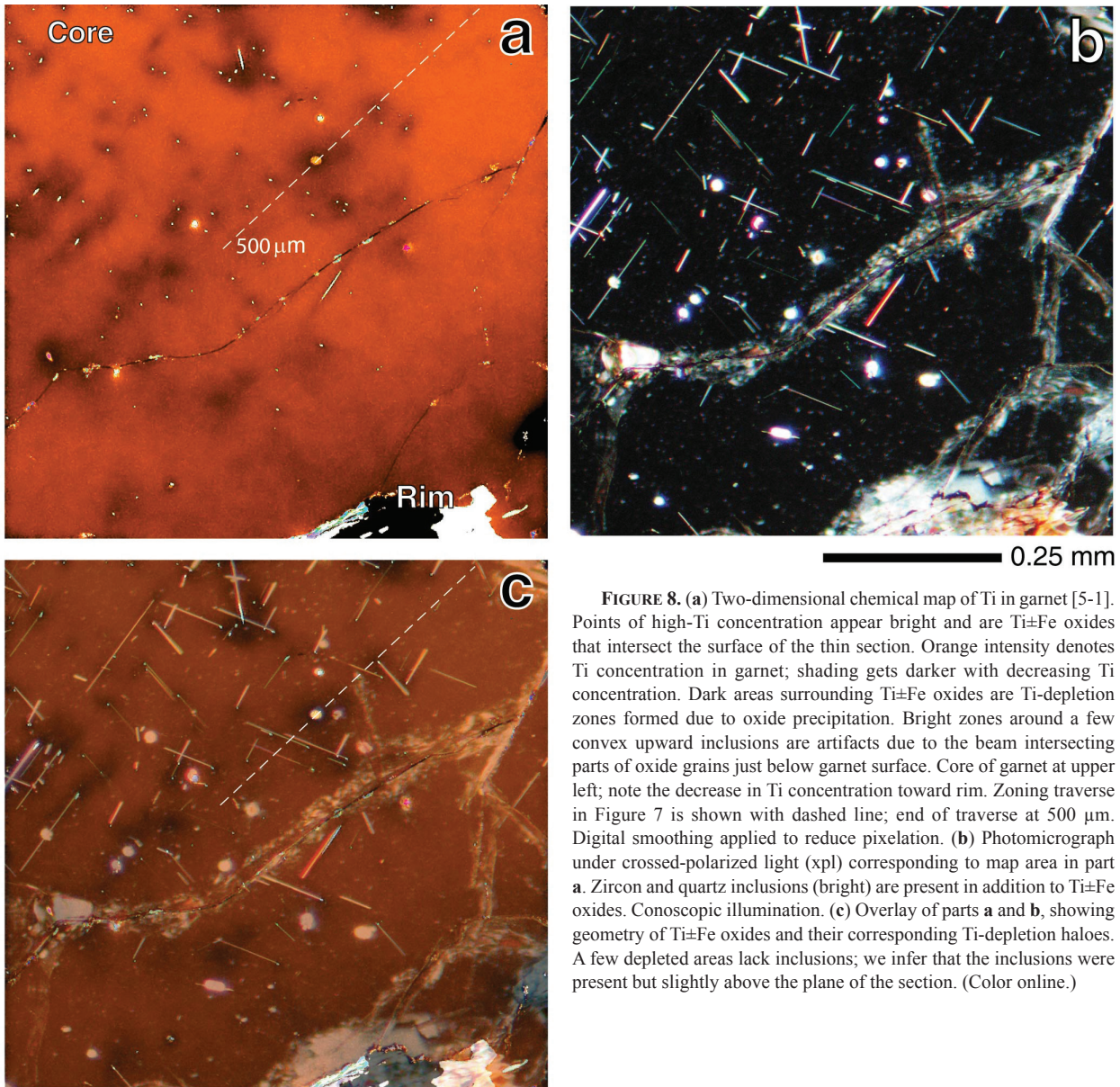
FIGURE 8. (a) Two-dimensional chemical map of Ti in garnet [5-1]. Points of high-Ti concentration appear bright and are Ti±Fe oxides that intersect the surface of the thin section. Orange intensity denotes Ti concentration in garnet; shading gets darker with decreasing Ti concentration. Dark areas surrounding Ti±Fe oxides are Ti-depletion zones formed due to oxide precipitation. Bright zones around a few convex upward inclusions are artifacts due to the beam intersecting parts of oxide grains just below garnet surface. Core of garnet at upper left; note the decrease in Ti concentration toward rim. Zoning traverse in Figure 7 is shown with dashed line; end of traverse at 500 μm. Digital smoothing applied to reduce pixelation. **(b)** Photomicrograph under crossed-polarized light (xpl) corresponding to map area in part **a**. Zircon and quartz inclusions (bright) are present in addition to Ti±Fe oxides. Conoscopic illumination. **(c)** Overlay of parts **a** and **b**, showing geometry of Ti±Fe oxides and their corresponding Ti-depletion haloes. A few depleted areas lack inclusions; we infer that the inclusions were present but slightly above the plane of the section. (Color online.)

rutile needles they studied lies either: (1) in the $(\bar{1}1\bar{1})_{Garnet}$ plane perpendicular to both the direction of rutile elongation and the $[\bar{1}1\bar{1}]$ garnet reference direction they used for plotting (crystals 1–6) or (2) very close to this plane (crystal 7). Ilmenite-garnet crystallographic relationships remain to be studied.

The above observations suggest that some type of crystallographic relationship between the garnet and rutile lattices exists. However, none of the seven studied rutile needles share exactly the same crystallographic orientation with respect to each other or the host garnet. Given this variability, Hwang et al. (2007) concluded that there is no *specific* crystallographic relationship between the rutile needles and their garnet hosts. This entails a partial to complete lack of lattice coherency between the phases (incoherency). Incoherent precipitates are widely known in materials science literature (e.g., Shewmon

1969), and have been found in some minerals as well, including feldspars (Putnis 1992).

Importantly, incoherent interfaces between garnet and rutile in no way preclude the precipitation hypothesis. Some examples of how such interfaces might develop are given here. During exsolution of coherent precipitates from a host crystal, there is lattice matching that minimizes surface energy (e.g., Putnis 1992). This can require some deformation of one or both of the lattice structures, resulting in considerable strain (e.g., Shewmon 1969). However, when tiny precipitates nucleate, it is generally thought that minimization of surface energy is more important than minimizing strain energy because the surface/volume ratio of a nucleus is large (strain energy is proportional to volume). Coherent precipitation is thus favored. On the other hand, as the precipitates grow, the surface free energy term becomes less
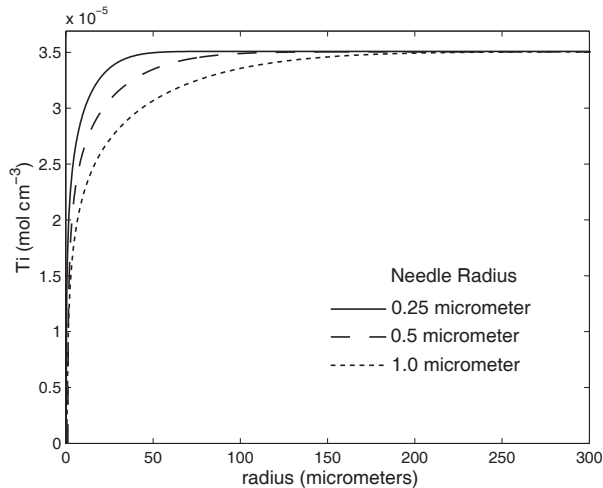
FIGURE 9. Model Ti-depletion halo profiles in garnet surrounding rutile needle at radius = 0 μm. Results shown for representative needle radii of 0.25, 0.5, and 1.0 μm.

important, and the precipitates may lose coherency to minimize lattice strains (e.g., Christian 1975). Another possibility is that the strain energy associated with deformation of the garnet and/or oxide lattices required to produce coherent precipitate nuclei exceeded the surface free energy penalty for incoherency, in spite of the large surface/volume. The very high tensile strength of garnet may have been important in this regard (cf. Karato 2008). In addition, we note that complete coherency is not always required to give the lowest energy interface between precipitate and host (Shewmon 1969). Furthermore, precipitates are known that have coherent or semi-coherent interfaces on some boundaries, and incoherent ones on others (e.g., Balluffi et al. 2005).

Griffin (2008) hypothesized that oriented rutile needles could originally have precipitated from garnet as the UHP TiO_2 polymorph with the α-PbO_2 structure (e.g., Hwang et al. 2000), which then inverted to rutile during exhumation. In this case, the original precipitates may have been coherent with the garnet lattice, prior to the phase transition to rutile. At present, we can neither confirm nor refute this exciting possibility, but emphasize that it is compatible with the evidence for a precipitation origin that we present.

Hwang et al. (2007), using AEM, observed a thin (1–2 nm) zone of amorphous material lying between rutile and garnet in the specimens they investigated. Further work is needed to document whether or not such zones exist in our specimens.

Garnet-chemical systematics

Given a precipitation origin for the Ti±Fe oxide needles, we posit that measured bulk Ti contents of garnet reflect the amount of Ti contained in garnet solid solution prior to precipitation. For garnet that lacks visible needles, or for which the needles are closely spaced, we estimated bulk Ti contents using an average of as many as 15 wide-beam (20 μm) analysis spots. For garnets in which the needles were more widely spaced, we used the wide-beam analysis grid approach described in the Methods section. The wide-beam integrated values are 0.12, 0.36, and 0.58 wt% TiO_2 for garnets in samples 5-1, 27-1, and

5-4, respectively. The full suite of elements was determined for garnet in 5-4 (284 individual analyses); it is illustrated in Figure 1e and its composition is given in Table 1 along with a range of other representative results.

The garnets are Mg rich (~25–35% pyrope) and contain considerable titanium. Manganese and Ca vary little and are present in relatively small amounts; it is likely that their concentrations were smoothed by diffusion during granulite-facies metamorphism (e.g., Tracy et al. 1976). TiO_2 contents range from <0.02 wt% in garnet rims to >0.5 wt% in the most needle-rich core regions. While the uncertainties associated with reintegrated EPMA analyses are well known (e.g., O'Brien and Rötzler 2003), the results nonetheless establish that garnets originally contained ~0.1 to ~0.6 wt% TiO_2. The values in the cores are considered to be minima, as there may have been diffusive loss of Ti to the garnet rims or perhaps even to the matrix during exhumation and cooling prior to needle precipitation (Fig. 6a).

As shown in Figures 10a and 10b, total Al in garnet clearly decreases as Ti or Ti+Cr increase, implying that these elements are related by substitution. Silicon plotted against Ti or Ti+Cr shows considerable scatter; nonetheless, the most Ti-rich garnet has the lowest Si (Figs. 10c and 10d). Notably, this garnet contains a large proportion of ilmenite needles (Fig. 1e; see below). Determining whether or not the Al-Ti-Cr relations involve octahedral sites, tetrahedral sites, or both, is hampered by the facts that tetrahedral Al is usually estimated by difference, is strongly dependent on site occupancy assignments, and is very sensitive to errors on silicon.

A different perspective on ^{VI}Al and its relationship with other elements can be obtained from analyses gathered along a profile across a single garnet of varying composition. Taking the profile in Figure 6 as an example, total Al decreases as Ti and Cr increase (Figs. 11a–11c). As the tetrahedral site is nearly filled with Si, there is almost certainly little ^{IV}Al (Fig. 11d). Consequently, the negative correlations between Al-Ti and Al-Cr are interpreted to reflect considerable substitution of Cr and Ti on octahedral sites. Although there is some scatter, a statistically significant negative correlation between Si and Ti exists (Fig. 11d). However, the total drop in Si with increasing Ti is small. No correlations are apparent between Ti or Cr and the sum of the eightfold site occupancies (~3 cations per 12 O atoms; not shown).

Garnet also contains small but measureable amounts of several minor and trace elements, including Zr, Cr, Y, P, and Na (Table 1). Good positive correlations between Na and Ti or Ti+Cr are evident (Figs. 10e and 10f). Zircon is present in very low abundances, but the highest concentrations (~150 ppm ZrO_2) are clearly found in the most Ti-rich garnets (Figs. 10g and 10h).

Substitution mechanisms

The substitution of ilmenite components on octahedral sites in garnet is easily described by the mechanism: $Fe^{2+}Ti^{4+} \leftrightarrow 2Al^{3+}$. Moreover, Van Roermund et al. (2000a) showed that precipitation of stoichiometric ilmenite probably requires original "supertitanic" garnet, analogous in many ways to supersilicic majorite, in which Ti is present on both octahedral and tetrahedral sites. Their model garnet composition is:

$$(Mg,Fe,Ca)_3\{(Al,Cr,Fe^{3+})_{2-2n}M^{2+}_n Ti_n\}(Si_{3-n}Ti_n)O_{12} \qquad (2)$$

where $0 < n < 1$ and M^{2+} is a divalent cation such as Mg, Fe, or Ca. Upon cooling and exhumation, this stoichiometry could decompose to produce coexisting Ti-poor garnet of "normal" composition ($M_3\{Al,Cr,Fe^{3+}\}_2Si_3O_{12}$), and ilmenite. Notably, the most ilmenite-rich garnet analyzed has high Ti and the lowest Al and Si, suggesting that substitutions similar to (2) affected both octahedral and tetrahedral sites (sample JAQ 5-4; Figs. 1e and 10a–10d; Table 1). This is also consistent with the negative correlations between Ti-Al and Ti-Si in Figure 11.

If Ti^{4+} originally resided only on tetrahedral sites in garnet coexisting with a silica polymorph, then the precipitation of rutile could occur by means of:

$$M_3Al_2Ti_3O_{12} + SiO_2 \rightarrow M_3Al_2Si_3O_{12} + TiO_2 \qquad (3)$$

(Massonne and Brandelik 1998; Massonne 2003).

Experimental data are limited, but available results suggest that this substitution is T sensitive. For example, Table 2 in Kawasaki and Motoyoshi (2007) indicates that most Ti was tetrahedrally coordinated in 1200–1300 °C, 1.5–2.0 GPa experiments. This is in contrast to octahedral substitutions that appear to be highly P sensitive. The 4–15 GPa, 1000–1400 °C experimental results of Zhang et al. (2003) are consistent with all Ti being octahedrally coordinated in garnet.

If at least some of the Ti for rutile precipitation in our samples resided on octahedral sites, which is highly likely, then the substitution mechanism is more complex because of charge-balance issues. Various mechanisms have been proposed, involving OH⁻, Na⁺, vacancies, redox state changes, or other crystallographic factors (cf. Van Roermund et al. 2000a; Khomenko et al. 1994; Zhang et al. 2003; Smith 2006; Proyer et al. 2009). The positive correlation between Na and Ti (Fig. 10) suggests mechanisms
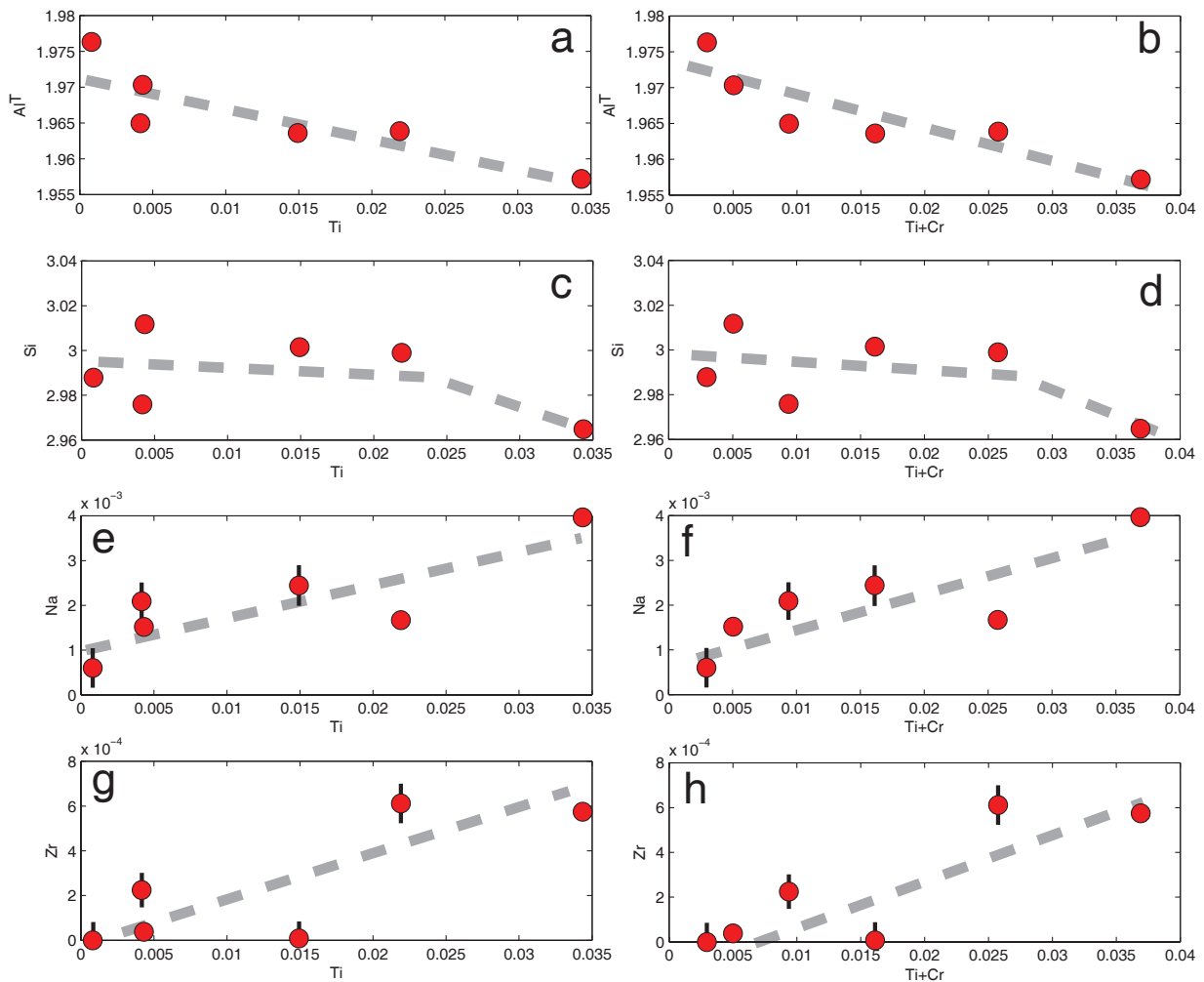

FIGURE 10. Geochemical relationships for range of garnet compositions given in Table 1: (a, b) Total Al (Al^T) vs. Ti and vs. Ti+Cr; (c, d) Si vs. Ti and vs. Ti+Cr; (e, f) Na vs. Ti and vs. Ti+Cr. 1σ errors on best-estimate Na values shown with black bars; some are smaller than the size of the data points. Correlations are statistically significant at p-values <0.05 (95% confidence). (g, h) Zr vs. Ti and vs. Ti+Cr. 1σ errors on best-estimate Zr values shown with black bars; some are smaller than the size of the data points. Zr vs. Ti+Cr correlation statistically significant at p-value <0.05 (95% confidence); Zr vs. Ti correlation has slightly poorer p-value of 0.055. (Color online.)
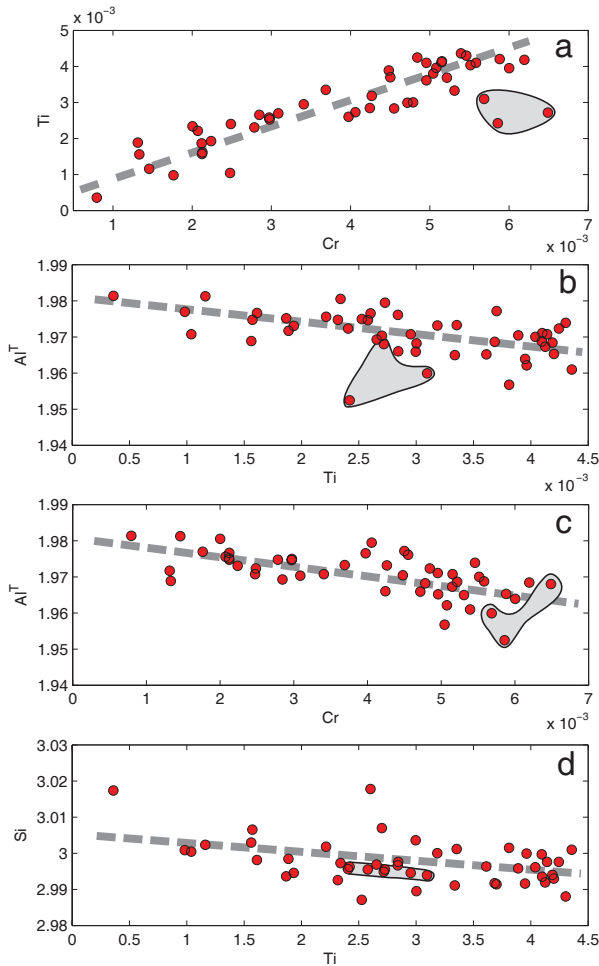
FIGURE 11. Geochemical relationships for garnet profiles shown in Figure 6. All correlations are statistically significant at p-values <0.01 (99% confidence). Gray-shaded areas correspond to Ti-depletion zone around rutile needle at x ~720 μm on profile. Formula units plotted on the basis of 12 O atoms: (**a**) Ti vs. Cr; (**b**) Al^T vs. Ti; (**c**) Al^T vs. Cr; (**d**) Si vs. Ti. (Color online.)

FIGURE 12. Survey of published P-T estimates for rocks containing garnets with oriented Ti±Fe oxide needle inclusions. T at maximum P (if known) is plotted. Arrows indicate that T or P estimate is a minimum. Uncertainties shown if given in original publication. Stars denote ilmenite needle-bearing garnets. Existing regional metamorphic P-T estimates for Acadian orogen in New England generalized from Carmichael (1978) and Spear (1993); some contact metamorphic rocks that reached higher temperatures are not shown. BM: diamondiferous felsic granulites, Bohemian Massif (Kröner et al. 2000; O'Brien and Rötzler 2003; Hwang et al. 2007; Kotková et al. 2011). C: garnet peridotites, Kolín area, central Czech Republic (Vrána 2008). E: Saxonian Erzgebirge, Saidenbach reservoir (Massonne 2003; Hwang et al. 2007). GR: Mantle garnet xenocrysts, Garnet Ridge, Arizona (Wang et al. 1999). H: Himalayan eclogite (Pandey et al. 2010). Ha: Hawaiian xenoliths (Keshav and Sen 2001; Keshav et al. 2007). J: Eclogite, Junan, Sulu UHP terrane (Zhang et al. 2003). K: Kulet whiteschist, Kokchetav Massif (Maruyama and Parkinson 2000; Shen et al. 2005). NQ: Garnet peridotite, North Qaidam, Tibetan Plateau (Song et al. 2004). O: Garnet peridotite, Otrøy, Western Gneiss Region, Norway (Van Roermund et al. 2000). PK: Eclogite xenoliths, Premier Kimberlite (Dludla et al. 2006). R: Garnet pyroxenite, Ronda, Spain (Obata 1994; Brueckner and Medaris 2000). Rh: Metapelitic rocks, Greek Rhodope (Mposkos and Kostopoulos 2001). Rz: Rizhao garnet clinopyroxenite, Sulu UHP terrane (Zhang and Liou 2003). S: Granulites from the Schwarzwald, Germany (Marschall et al. 2003). P-T estimate is a minimum. SB: High-pressure granulite, Snowbird tectonic zone, Canada (Snoeyenbos et al. 1995). P-T estimate is a minimum. WGR: Felsic granulite, Western Gneiss Region, Norway (Larsen et al. 1998). Y: Yangkou ultramafic-mafic complex, Sulu UHP terrane (Zhang et al. 2003). (Color online.)

of the form: $Na^+Ti^{4+} \leftrightarrow M^{2+}Al^{3+}$. However, the amount of Na is insufficient to account for all the excess Ti charge. Although the mechanism(s) for rutile precipitation remains to be precisely constrained, the FEG-EPMA results leave little doubt that rutile precipitated from Ti-bearing garnet.

Former majoritic garnets from UHP and mantle garnet peridotite settings commonly contain rod-shaped pyroxene precipitates, together with other phases, including rutile needles and rods of quartz or apatite (e.g., Zhang and Liou 1999; Van Roermund et al. 2000b; Pandey et al. 2010). The pyroxenes and quartz reflect substitutions in the original garnet, which place Si on octahedral sites, such as $(Ca,Fe,Mg)^{2+}Si^{4+} \leftrightarrow 2Al^{3+}$; thus total Si exceeds 3 atoms per 12 O atoms in majorite. The operation of such substitutions in our rocks is in doubt, as we have found only one inclusion of orthopyroxene in all the garnets studied. It is important to note, however, that in the experiments of Zhang et al. (2003), high Si contents well in excess of 3 atoms per formula unit were only attained at $P > $~4–5 GPa. Consequently,
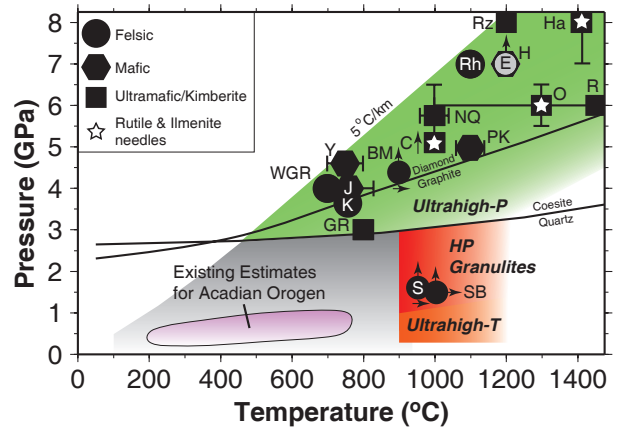
the garnets studied here could have formed at quite high P and still not have contained much excess silica.

It is also tempting to speculate that the "boxy" quartz inclusions represent some form of silica precipitation from garnet (Fig. 5). Smith (2006) proposed that the following "supersiligar" mechanism could produce supersilicic garnet: $^{VIII}(Mg^{2+})^{VI}(Mg^{2+}) \leftrightarrow {}^{VIII}\square{}^{VI}(Si^{4+})$, where $\square$ denotes a vacancy (presumably Fe^{2+} or other divalent cations could take the place of Mg). Smith showed that decomposition of such a phase could potentially yield garnet together with a silica polymorph, and hypothesized that this may be the origin of quartz or coesite inclusions in some exhumed UHP garnets. The close association of quartz inclusions and apatite rods in our rocks may represent some form of co-precipitation mechanism (Fig. 5). The necessary Si,

Ca, and P could enter the garnet structure via: $Na^+P^{5+} \leftrightarrow Ca^{2+}Si^{4+}$ (Zhang et al. 2003).

CONCLUDING REMARKS

Our results document a precipitation origin for oriented rutile and ilmenite in garnet cores from the Merrimack synclinorium, northeastern Connecticut. Of course, other mechanisms, such as those discussed by Hwang et al. (2007), may have operated in other rocks from different tectonic settings. The precipitates almost certainly formed from Ti-bearing garnet during exhumation and cooling. Original TiO_2 contents exceeded ~0.5 wt% in some garnets. Available experimental and field evidence shows that such high-Ti garnet forms only under UHP/mantle conditions, or under granulite conditions at T of at least ~900–1000 °C (~0.3 wt% to >1 wt%; e.g., Ono 1998; Zhang et al. 2003; Kawasaki and Motoyoshi 2007). Analyzed natural garnets from these environments often retain several tenths of a wt% TiO_2 or more, comparable to the amounts measured in this study (cf. Massonne 2003; Marschall et al. 2003; Vrána 2008; Pandey et al. 2010).

A survey of published data on rocks containing garnets with abundant Ti±Fe oxide needles or rutile bicrystals shows that, regardless of protolith, those whose maximum pressures can be estimated reached ultrahigh pressures above the quartz-coesite transition (Fig. 12). Furthermore, over 90% of these were at or within the diamond stability field.

Other mineralogical observations also point to extreme conditions of crystallization. For instance, srilankite has been found in eclogites, granulites, and kimberlites (Troitzsch and Ellis 2004). Moreover, to our knowledge, coexisting srilankite and crichtonite inclusions (Figs. 3c and 3d) are known only from mantle garnet from Garnet Ridge, Arizona, U.S.A. (Wang et al. 1999); crichtonite without srilankite has also been found in garnet peridotites from the central Czech Republic (Vrána 2008). In both of these examples, the rare oxides coexist with rutile needles, as is the case for the rocks studied herein. Srilankite + rutile has been synthesized experimentally at 1440 °C and 2.8 GPa (Troitzsch and Ellis 2004). In addition, ilmenite needles in garnet are known almost exclusively from rocks that experienced mantle P-T conditions (Fig. 12). The rutile microbicrystal morphology (Fig. 4) has been reported from the UHP Kokchetav whiteschists and microdiamond-bearing Erzgebirge rocks (Hwang et al. 2000; Shen et al. 2005). Apatite rods have been discovered in several UHP settings, and are present in the Connecticut rocks as well (Fig. 5; Ye et al. 2000; Mposkos and Kostopoulos 2001; Zhang et al. 2003). The significant proportion of OH⁻ in the apatite is unusual for high-grade rocks, but is consistent with apatite chemistry in the UHP rocks of the Greek Rhodope (Mposkos and Kostopoulos 2001).

The elevated concentrations of key trace elements in garnet and rutile also suggest extreme P and/or T. For example, garnet Zr contents of ~100 ppm are comparable to those measured in granulite xenoliths from the lower crust (Villaseca et al. 2007). Positive correlations between Na and Ti are observed in the Connecticut rocks (Fig. 10) as well as in garnet peridotites (Vrána 2008). The presence of Na is characteristic of high P-T garnets; the measured Na_2O values between ~0.01 and 0.03 wt% are comparable to those found in garnets from a wide range of eclogites, garnet peridotites, and mantle xenoliths (Sobolev and Lavrent'ev

1971; Vrána 2008). Finally, ZrO_2 contents in rutile coexisting with a silica polymorph that approach the weight percent level indicate extremely high-T of formation in excess of 900 °C regardless of pressure (Tomkins et al. 2007); the geochemical systematics of the rutile will be addressed in a separate paper.

The inferred extreme P and/or T metamorphism predated both the granulite facies mineral assemblages preserved in the rock matrix, and the later kyanite zone overprint. Rodgers (1981) interpreted the synclinorium to be the deep roots of an accretionary prism that formed during Late Ordovician through Early Devonian subduction along the ancient eastern margin of North America prior to collision with Avalonian basement. It is possible that the Ti±Fe oxide-bearing garnet cores represent the deeply exhumed roots of this subduction-collision complex. Considerable work is now required to determine the P-T history of metamorphism and its petrogenetic implications. The presence of extreme P and/or T rocks in the Acadian orogen may force a re-evaluation of tectonic models for the region.

REFERENCES CITED

Ague, J.J. (1994) Mass transfer during Barrovian metamorphism of pelites, south-central Connecticut, II: Channelized fluid flow and the growth of staurolite and kyanite. American Journal of Science, 294, 1061–1134.
——— (1996) Deep crustal growth of quartz, kyanite, and garnet into large-aperture, fluid-filled fractures, north-eastern Connecticut, USA. Journal of Metamorphic Geology, 13, 299–314.
——— (2011) Extreme channelization of fluid and the problem of element mobility during Barrovian metamorphism. American Mineralogist, 96, 333–352.
Armstrong, T.R., Tracy, R.J., and Hames, W.E. (1992) Contrasting styles of Taconian, eastern Acadian, and western Acadian metamorphism, central and western New England. Journal of Metamorphic Geology, 10, 415–426.
Balluffi, R.W., Allen, S.M., and Carter, W.C. (2005) Kinetics of Materials, 645 p. Wiley-Interscience, Hoboken, New Jersey.
Barron, B.J., Barron, L.M., and Duncan, G. (2005) Eclogitic and ultrahigh-pressure crustal garnets and their relationship to Phanerozoic subduction diamonds, Bingara area, New England Fold Belt, eastern Australia. Economic Geology, 100, 1565–1582.
Bence, A.E. and Albee, A.L. (1968) Empirical correction factors for the electron microanalysis of silicates and oxides. Journal of Geology, 76, 382–403.
Brueckner, H.K. and Medaris, L.G. (2000) A general model for the intrusion and evolution of 'mantle' garnet peridotites in high-pressure and ultra-high-pressure metamorphic terranes. Journal of Metamorphic Geology, 18, 123–133.
Carmichael, D.M. (1978) Metamorphic bathozones and bathograds: a measure of post-metamorphic uplift and erosion on a regional scale. American Journal of Science, 278, 769–797.
Christian, J.W. (1975) The Theory of Transformations in Metals and Alloys, 2nd ed., 586 p. Pergamon Press, Oxford, U.K.
Dludla, S., le Roex, A.P., and Gurney, J.J. (2006) Eclogite xenoliths from the Premier kimberlite, South Africa: geochemical evidence for a subduction origin. South African Journal of Geology, 109, 353–368.
Dobrzhinetskaya, L.F., Wirth, R., and Green, H.W. II (2007) A look inside of diamond-forming media in deep subduction zones. Proceedings of the National Academy of Sciences, 104, 9128–9132.
Ernst, W.G. and Liou, J.G. (2008) High- and ultrahigh-pressure metamorphism: Past results and future prospects. American Mineralogist, 93, 1771–1786.
Fahey, R.J. and Pease, M.H. Jr. (1977) Preliminary bedrock geologic map of the South Coventry quadrangle, Tolland County, Connecticut. U.S. Geological Survey Open-File Report, 77–584.
Frezzotti, M.L., Selverstone, J., Sharp, Z.D., and Compagnoni, R. (2011) Carbonate dissolution during subduction revealed by diamond-bearing rocks from the

Alps. Nature Geoscience, 4, 703–706.

Griffin, W.L. (2008) Major transformations reveal Earth's deep secrets. Geology, 36, 95–96.

Griffin, W.L., Jensen, B.B., and Misra, S.N. (1971) Anomalously elongated rutile in eclogite-facies pyroxene and garnet. Norsk Geologisk Tidsskrift, 51, 177–185.

Hacker, B.R., Sharp, T., Zhang, R.Y., Liou, J.G., and Hervig, R.L. (1997) Determining the origin of ultrahigh-pressure lherzolites. Science, 278, 702–704.

Hacker, B.R., Calvert, A., Zhang, R.Y., Ernst, W.G., and Liou, J.G. (2003) Ultrarapid exhumation of ultrahigh-pressure diamond-bearing metasedimentary rocks of the Kokchetav Massif, Kazakhstan? Lithos, 70, 61–75.

Hwang, S.L., Shen, P., Chu, H.T., and Yui, T.F. (2000) Nanometer-size α-PbO$_2$-type TiO$_2$ in garnet: A thermobarometer for ultrahigh-pressure metamorphism. Science, 288, 321–324.

Hwang, S.L., Yui, T.F., Chu, H.T., Shen, P., Schertl, H.P., Zhang, R.Y., and Liou, J.G. (2007) On the origin of oriented rutile needles in garnet from UHP eclogites. Journal of Metamorphic Geology, 25, 349–362.

Karato, S. (2008) Deformation of Earth Materials: An introduction to the rheology of solid Earth, 474 p. Cambridge University Press, U.K.

Kawasaki, T. and Motoyoshi, Y. (2007) Solubility of TiO$_2$ in garnet and orthopyroxene: Ti thermometer for ultrahigh-temperature granulites. U.S. Geological Survey and The National Academies; USGS OF-2007-1047, Short Research Paper 038; DOI: 10.3133/of2007-1047.srp038.

Keshav, S. and Sen, G. (2001) Majoritic Garnets in Hawaiian xenoliths: Preliminary results. Geophysical Research Letters, 28, 3509–3512.

Keshav, S., Sen, G., and Presnall, D.C. (2007) Garnet-bearing xenoliths from Salt Lake Crater, Oahu, Hawaii: High-pressure fractional crystallization in the oceanic mantle. Journal of Petrology, 48, 1681–1724.

Khomenko, V.M., Langer, K., Beran, A., Koch-Müller, M., and Fehr, T. (1994) Titanium substitution and OH-Bearing defects in hydrothermally grown pyrope crystals. Physics and Chemistry of Minerals, 20, 483–488.

Kotková, J., O'Brien, P.J., and Ziemann, M.A. (2011) Diamond and coesite discovered in Saxony-type granulite: Solution to the Variscan garnet peridotite enigma. Geology, 39, 667–670.

Koziol, A.M. and Snoeyenbos, D. (2009) Minor element solid solution in garnet at ultra-high pressure metamorphic conditions. Geological Society of America Abstracts with Programs, 41(7), 636.

Kröner, A., O'Brien, P.J., Nemchin, A.A., and Pidgeon, R.T. (2000) Zircon ages for high pressure granulites from South Bohemia, Czech Republic, and their connection to Carboniferous high temperature processes. Contributions to Mineralogy and Petrology, 138, 127–142.

Kvenvolden, K.A. and Roedder, E. (1971) Fluid inclusions from quartz crystals in South-West Africa. Geochimica et Cosmochimica Acta, 35, 1209–1214.

Larsen, R.B., Eide, E.A., and Burke, E.A.J. (1998) Evolution of metamorphic volatiles during exhumation of microdiamond-bearing granulites in the Western Gneiss Region, Norway. Contributions to Mineralogy and Petrology, 133, 106–121.

Mallmann, G., O'Neill, H.St.C., and Klemme, S. (2009) Heterogeneous distribution of phosphorus in olivine from otherwise well-equilibrated spinel peridotite xenoliths and its implications for the mantle geochemistry of lithium. Contributions to Mineralogy and Petrology, 158, 485–504.

Marschall, H.R., Kalt, A., and Hanel, M. (2003) P-T evolution of a Variscan lower-crustal segment: a study of granulites from the Schwarzwald, Germany. Journal of Petrology, 44, 227–253.

Maruyama, S. and Parkinson, C.D. (2000) Overview of the geology, petrology and tectonic framework of the high-pressure–ultrahigh-pressure metamorphic belt of the Kokchetav Massif, Kazakhstan. The Island Arc, 9, 439–455.

Massonne, H.J. (2003) A comparison of the evolution of diamondiferous quartz-rich rocks from the Saxonian Erzgebirge and the Kokchetav Massif: are so-called diamondiferous gneisses magmatic rocks? Earth and Planetary Science Letters, 216, 347–364.

Massonne, H.J. and Brandelik, A. (1998) Ti in Al-garnet—a newly calibrated geothermobarometer for HP and UHP metamorphic rocks. EOS, 79, F972.

Meinhold, G. (2010) Rutile and its applications in earth sciences. Earth-Science Reviews, 102, 1–28.

Moraes, R., Brown, M., Fuck, R.A., Camargo, M.A., and Lima, T.M. (2002) Characterization and P-T evolution of melt-bearing ultrahigh-temperature granulites: an example from the Anápolis-Itauçu complex of the Brasília fold belt, Brazil. Journal of Petrology, 43, 1673–1705.

Mposkos, E.D. and Kostopoulos, D.K. (2001) Diamond, former coesite and supersilicic garnet in metasedimentary rocks from the Greek Rhodope: a new ultrahigh-pressure metamorphic province established. Earth and Planetary Science Letters, 192, 497–506.

Obata, M. (1994) Material transfer and local equilibria in a zoned kelyphite from a garnet pyroxenite, Ronda, Spain. Journal of Petrology, 35, 271–287.

O'Brien, P.J. and Rötzler, J. (2003) High-pressure granulites: formation, recovery of peak conditions and implications for tectonics. Journal of Metamorphic Geology, 21, 3–20.

O'Brien, P.J., Kröner, A., Jaeckel, P., Hegner, E., Żelaźniewicz, A., and Kryza, R. (1997) Petrological and isotopic studies on Palaeozoic high-pressure granulites,

Góry Sowie Mts, Polish Sudetes. Journal of Petrology, 38, 433–456.

Ono, S. (1998) Stability limits of hydrous minerals in sediment and mid-ocean ridge basalt compositions. Implications for water transport in subduction zones. Journal of Geophysical Research, 103, 18253–18267.

Pandey, A., Leech, M., Milton, A., Singh, P., and Verma, P.K. (2010) Evidence of former majoritic garnet in Himalayan eclogite points to 200-km-deep subduction of Indian continental crust. Geology, 38, 399–402.

Peper, J.D. and Pease, M.H. Jr. (1975) Geologic map of the Westford quadrangle, Connecticut. U.S. Geological Survey Quadrangle Map, GQ-1214.

Proyer, A., Krenn, K., and Hoinkes, G. (2009) Oriented precipitates of quartz and amphibole in clinopyroxene of metabasites from the Greek Rhodope: a product of open system precipitation during eclogite–granulite–amphibolite transition. Journal of Metamorphic Geology, 27, 639–654.

Putnis, A. (1992) Introduction to Mineral Sciences. Cambridge University Press, U.K.

Robinson, P. and Tucker, R.D. (1982) The Merrimack synclinorium in northeastern Connecticut. American Journal of Science, 282, 1735–1744.

Robinson, P., Terry, M.P., Carswell, T., Van Roermund, H., Krogh, T.E., Root, D., Tucker, R.D., and Solli, A. (2003) Tectono-stratigraphic setting, structure, and petrology of HP and UHP metamorphic rocks and garnet peridotites in the Western Gneiss Region, Møre and Romsdal, Norway. Geological Survey of Norway, Report no. 2003.057, 107–113.

Rodgers, J. (1981) The Merrimack synclinorium in northeastern Connecticut. American Journal of Science, 281, 176–186.

——— (1985) Bedrock Geological Map of Connecticut, scale 1:125,000. Connecticut Geological and Natural History Survey, Department of Environmental Protection, Hartford, Connecticut.

Schumacher, J.C., Schumacher, R., and Robinson, P. (1989) Acadian metamorphism in central Massachusetts and southwestern New Hampshire: evidence for contrasting P-T trajectories. In J.S. Daly, R.A. Cliff, and B.W.D. Yardley, Eds., Evolution of Metamorphic Belts, 34, p. 453–460. Geological Society Special Publication, London.

Shau, Y.H., Yang, H.Y., and Peacor, D.R. (1991) On oriented titanite and rutile inclusions in biotite. American Mineralogist, 76, 1205–1217.

Shen, P., Hwang, S.L., Chu, H.T., Yui, T.F., Pan, C., and Huang, W.L. (2005) On the transformation pathways of α-PbO$_2$-type TiO$_2$ at the twin boundary of rutile bicrystals and the origin of rutile bicrystals. European Journal of Mineralogy, 17, 543–552.

Shewmon, P.G. (1969) Transformations in Metals, 394 p. McGraw-Hill, New York.

Smith, D.C. (2006) The SHAND quaternary system for evaluating the supersilicic or subsilicic crystal-chemistry of eclogite minerals, and potential new UHPM pyroxene and garnet end-members. Mineralogy and Petrology, 88, 87–122.

Snoeyenbos, D.R. and Koziol, A. (2008) Exsolution phenomena of UHP type in garnets From Western New England, USA. Eos, American Geophysical Union, V31E-07.

Snoeyenbos, D.R., Williams, M.L., and Hanmer, S. (1995) Archean high-pressure metamorphism in the western Canadian Shield. European Journal of Mineralogy, 7, 1251–1272.

Sobolev, N.V. Jr. and Lavrent'ev, Y.G. (1971) Isomorphic sodium admixture in garnets formed at high pressures. Contributions to Mineralogy and Petrology, 31, 1–12.

Song, S., Zhang, L., and Niu, Y. (2004) Ultra-deep origin of garnet peridotite from the North Qaidam ultrahigh-pressure belt, northern Tibetan Plateau, NW China. American Mineralogist, 89, 1330–1336.

Spear, F.S. (1993) Metamorphic Phase Equilibria and Pressure-Temperature-Time Paths, 1, 799 p. Monograph, Mineralogical Society of America, Chantilly, Virginia.

Thomas, J.W. (1995) Numerical Partial Differential Equations: Finite Difference Methods, 437 p. Springer-Verlag, New York.

Thomson, J.A. (2001) A counterclockwise P-T path for anatectic pelites, south-central Massachusetts. Contributions to Mineralogy and Petrology, 141, 623–641.

Tomkins, H.S., Powell, R., and Ellis, D.J. (2007) The pressure dependence of the zirconium-in-rutile thermometer. Journal of Metamorphic Geology, 25, 703–713.

Tracy, R.J., Robinson, P., and Thompson, A.B. (1976) Garnet composition and zoning in the determination of temperature and pressure of metamorphism, central Massachusetts. American Mineralogist, 61, 762–775.

Troitzsch, U. and Ellis, D.J. (2004) High-PT study of solid solutions in the system ZrO$_2$-TiO$_2$: The stability of srilankite. European Journal of Mineralogy, 16, 577–584.

Van Roermund, H.L.M. and Drury, M.R. (1998) Ultra-high pressure ($P > 6$ GPa) garnet peridotites in Western Norway: Exhumation of mantle rocks from >185 km depth. Terra Nova, 10, 295–301.

Van Roermund, H.L.M., Drury, M.R., Barnhoorn, A., and de Ronde, A. (2000a) Non-silicate inclusions in garnet from an ultra-deep orogenic peridotite. Geological Journal, 35, 209–229.

——— (2000b) Super-silicic garnet microstructures from an orogenic garnet peridotite, evidence for an ultra-deep (>6 GPa) origin. Journal of Metamorphic

Geology, 18, 135–147.

Villaseca, C., Orejana, D., and Paterson, B.A. (2007) Zr–LREE rich minerals in residual peraluminous granulites, another factor in the origin of low Zr–LREE granitic melts? Lithos, 96, 375–386.

Vrána, S. (2008) Mineral inclusions in pyrope from garnet peridotites, Kolín area, central Czech Republic. Journal of Geosciences, 53, 17–30.

Wang, L., Essene, E.J., and Zhang, Y. (1999) Mineral inclusions in pyrope crystals from Garnet Ridge, Arizona, USA: implications for processes in the upper mantle. Contributions to Mineralogy and Petrology, 135, 164–178.

Watson, E.B., Wark, D.A., and Thomas, J.B. (2006) Crystallization thermometers for zircon and rutile. Contributions to Mineralogy and Petrology, 151, 413–433.

Wintsch, R.P., Sutter, J.F., Kunk, M.J., Aleinikoff, J.N., and Dorais, M.J. (1992) Contrasting *P-T-t* paths: Thermochronologic evidence for a late Paleozoic final assembly of the Avalon composite terrane in the New England Appalachians. Tectonics, 11, 672–689.

Ye, K., Cong, B., and Ye, D. (2000) The possible subduction of continental material to depths greater than 200 km. Nature, 407, 734–736.

Zack, T., Moraes, R., and Kronz, A. (2004) Temperature dependence of Zr in rutile: empirical calibration of a rutile thermometer. Contributions to Mineralogy and Petrology, 148, 471–488.

Zhang, R.Y. and Liou, J.G. (1999) Exsolution lamellae in minerals from ultrahigh-pressure rocks. International Geology Review, 41, 981–993.

——— (2003) Clinopyroxenite from the Sulu ultrahigh-pressure terrane, eastern China: Origin and evolution of garnet exsolution in clinopyroxene. American Mineralogist, 88, 1591–1600.

Zhang, R.Y., Zhai, S.M., Fei, Y.W., and Liou, J.G. (2003) Titanium solubility in co-existing garnet and clinopyroxene at very high pressure: the significance of exsolved rutile in garnet. Earth and Planetary Science Letters, 216, 591–601.